POLITECNICO DI TORINO
Repository ISTITUZIONALE

Bandwidth and Power Back-Off Performances of a Class-EM/F3 Power Amplifier

Original
Bandwidth and Power Back-Off Performances of a Class-EM/F3 Power Amplifier / Mugisho, M.S., Thian, M., Piacibello, A., Camarchia, V., Quay, R.. - (2021), pp. 362-365. (51st European Microwave Conference, EuMC 2021 London (UK) 04-06 April 2022) [10.23919/EuMC50147.2022.9784237].

Availability:
This version is available at: 11583/3017385 since: 2026-11-04T08:40:27Z

Publisher:
IEEE

Published
DOI:10.23919/EuMC50147.2022.9784237

Terms of use:

This article is made available under terms and conditions as specified in the corresponding bibliographic description in the repository

Publisher copyright
IEEE postprint/Author's Accepted Manuscript

©2021 IEEE. Personal use of this material is permitted. Permission from IEEE must be obtained for all other uses, in any current or future media, including reprinting/republishing this material for advertising or promotional purposes, creating new collecting works, for resale or lists, or reuse of any copyrighted component of this work in other works.

(Article begins on next page)

10 November 2026

Bandwidth and Power Back-Off Performances of a Class-E_M/F_3 Power Amplifier

Moïse Safari Mugisho[1], Mury Thian[2], Anna Piacibello[3], Vittorio Camarchia[4], Rüdiger Quay[5]
[1,5]Fraunhofer Institute for Applied Solid-State Physics (IAF), 79108 Freiburg, Germany
[3]Microwave Engineering Center for Space Applications (MECSA), 00133 Rome, Italy
[3,4]Politecnico di Torino, 10129 Turin, Italy
{[1]moise.safari, [5]ruediger.quay}@iaf.fraunhofer.de, {[3]anna.piacibello, [4]vittorio.camarchia}@polito.it

***Abstract*— This paper presents the design of a broadband high-efficiency Class-E_M/F_3 power amplifier (PA). The PA exhibits a significantly reduced peak drain voltage compared to its predecessor (Class E_M) and a large fractional bandwidth of 34.3% at peak power as well as 6 dB output back-off power (OBO) while satisfying the zero voltage switching, zero voltage derivative switching, zero current switching, and zero current derivative switching conditions to minimize power dissipation within the active device. A Class-E_M/F_3 PA employing a transmission-line load network was proposed and implemented using GaN HEMTs. The PA exhibits a drain efficiency (*DE*) of 77%, a power-added efficiency (*PAE*) of 72% at a peak output power (P_{out}) of 42.1 dBm at 1.8 GHz. With P_{out} backed-off by 6 dB, the PA delivers a *DE* of 41% and a *PAE* of 40%. Across a frequency range from 1.4 to 2 GHz, the PA delivers *DE* > 67%, *PAE* > 58%, and a P_{out} of 41.2 ± 1 dBm. At 6-dB OBO, the PA delivers *DE* > 39%, a *PAE* > 34%, and a P_{out} of 35 ± 1.2 dBm.**

Keywords— 5G, broadband, Class-E_M, Class-E_M/F_3, harmonic injection, high efficiency, power back-off.

I. Introduction

Modern wireless communication systems such as 5G require PAs with a high efficiency over a wide frequency range at both peak power (PP) and back-off power (OBO). The bandwidth characteristics of conventional high-efficiency PAs such as the Class E [1], Inverse Class E [2], Class F [3], and Inverse Class F [4] are hindered by the open and short circuit harmonic terminations adopted in the load-networks thereof. To address the bandwidth limitation of the foregoing PAs, high-efficiency continuous-mode PAs with resistive-reactive load terminations at the fundamental (f_0) and second harmonic frequency ($2f_0$) were introduced in [5]-[7]. However, the continuous-mode PAs deliver a broadband high efficiency only at PP. Hence they are not suitable for 5G applications, where a broadband high-efficiency operation is also required at OBO. In [8], it was shown that the harmonic-injection Class-E_M PA inherits the broadband characteristic of continuous-mode PAs due to its resistive-reactive terminations at f_0 and $2f_0$. However, the high peak switch voltage of the Class-E_M PA in [8], i.e., $4.4\times V_{DD}$ compared to $3.6\times V_{DD}$ of the Class-E's hinders the widespread usage thereof. Nonetheless, the high peak switch voltage of the Class-E_M PA was significantly reduced in [9], where the third-harmonic short-circuit termination of the Inverse Class-F PA was adopted in the load network of the Class-E_M PA resulting in a novel topology called the Class-E_M/F_3 PA.

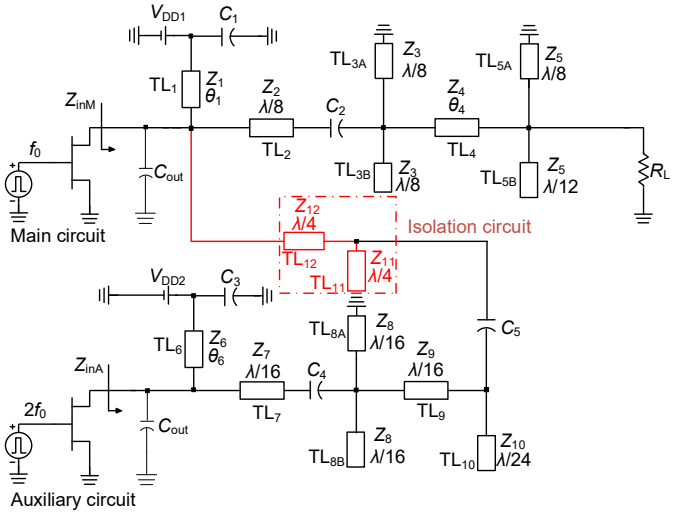


Fig. 1. Transmission-line load network of the proposed Class-E_M/F_3 PA.

In this paper, we will show that in addition to the reduced peak switch voltage, the Class-E_M/F_3 also retains the broadband characteristic of its predecessor, i.e., Class E_M owing to its resistive-reactive termination at f_0 and $2f_0$. Furthermore, it will be shown that the broadband high-efficiency operation is obtained not only at PP but also at 6-dB BOP. Hence, these inherent characteristics of the Class-E_M/F_3 PA render it a suitable candidate for 5G applications. These claims are sustained through the design, simulation, and implementation of a GaN HEMTs Class-E_M/F_3 PA operating from 1.4 to 2 GHz, thus suitable for the 5G NR FR1 applications.

II. Design of a Transmission-Line Class-E_M/F_3 PA

The basic operating principle and circuit analysis of the Class-E_M/F_3 PA are reported in [9]. The isolation circuit allows the main and auxiliary circuits to interact only at $2f_0$ while being isolated at f_0 and $3f_0$. Here, we present the design of a transmission-line Class-E_M/F_3 PA using Wolfspeed's CGH40010F GaN HEMTs with an intrinsic output capacitance (C_{out}) of 1.27 pF. The proposed transmission-line load network is shown in Fig. 1, wherein the shorted stub TL_1 of the main circuit (or TL_6 of the auxiliary circuit) and the output

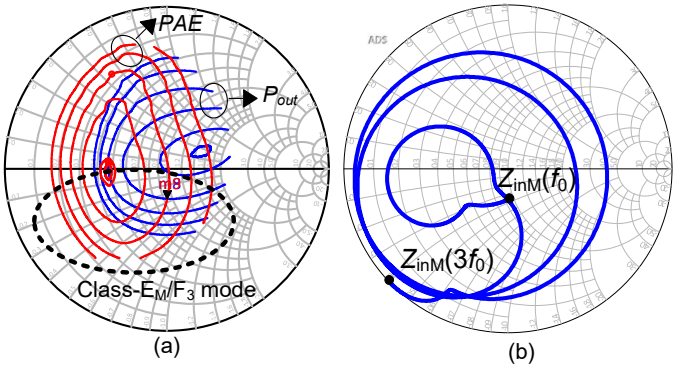


Fig. 2. (a) Simulated load-pull contours. (b) Simulated main circuit's load-network impedance at f_0 and $3f_0$.

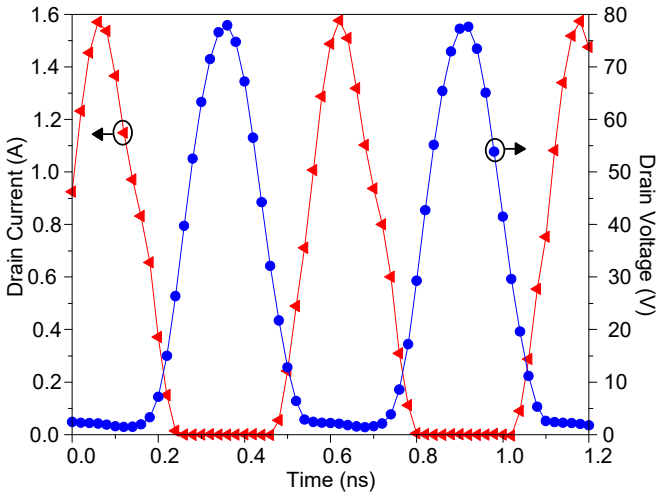


Fig. 3. Simulated drain current and voltage waveforms of the main circuit using the actual transistor large-signal model at 1.8 GHz.

capacitance of the active device C_{out} form a parallel resonant circuit. Thus, the characteristic impedances Z_1 and Z_6 and the electrical lengths θ_1 and θ_6 can be computed such that the parallel circuit formed by TL_{L1} and C_{out} on the main circuit is tuned at f_0, and the parallel circuit formed by TL_6 and C_{out} on the auxiliary circuit is tuned at $2f_0$. Consequently, C_{out} is absorbed into the transmission-line load network and the deleterious effect thereof on the PA's operating bandwidth is minimized. Additionally, the parallel resonant circuit TL_{L1}–C_{out} presents a low impedance to the drain of the main device at $3f_0$. The characteristic impedances $Z_2 = Z_4$, Z_5, and the electrical length θ_2 can be calculated to match the load resistance R_L to the optimum impedance obtained from load-pull simulation. This approach can be adopted for the design of the auxiliary circuit as well but the discussion hereinafter is focused on the main circuit for the sake of brevity.

The simulated P_{out} and PAE contours are shown in Fig. 2(a), where the region corresponding to the Class-E_M/F_3 mode, i.e., the region with capacitive load impedance at f_0 is highlighted. An optimum load impedance (Z_{opt}) of 47.5 – j13 Ω was extracted at the drain of the main device at 1.75 GHz. The characteristic impedances of TL_2/TL_4 and TL_{5A}/TL_{5B}, i.e., $Z_2 = Z_4 = 48.5$ Ω and $Z_5 = 55$ Ω were calculated to match $R_L = 50$ Ω to Z_{opt} for a selected $\theta_4 = \lambda/8$ at f_0.

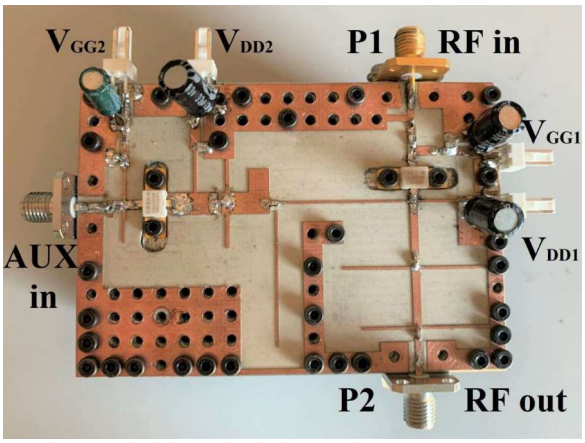


Fig. 4. Photograph of the realized Class-E_M/F_3 PA.

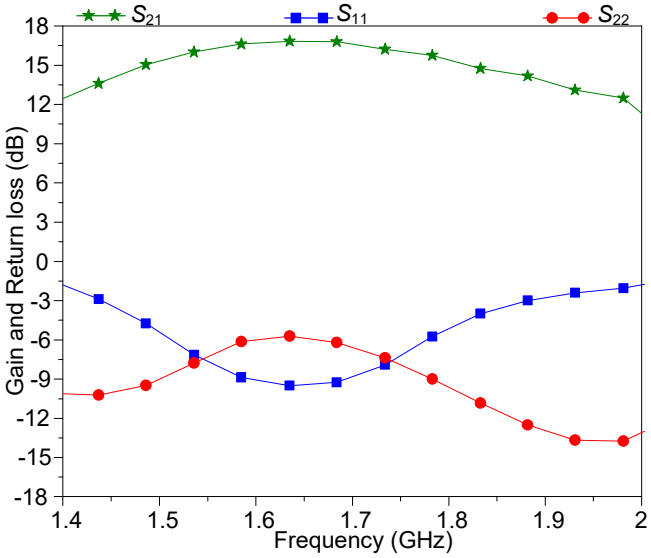


Fig. 5. Measured scattering parameters.

The simulated impedance of the load network (Z_{inM}) is plotted in Fig. 2(b) showing that $Z_{inM} = Z_{opt}$ at f_0 and Z_{inM} is low enough at $3f_0$. Thus, the proposed transmission-line load network satisfies the impedance- termination requirements of the Class-E_M/F_3.

The designed Class-E_M/F_3 PA was implemented with microstrip lines, a printed circuit board (PCB) layout was generated using ADS, and subsequently Momentum EM simulations were performed on the PCB layout. Shown in Fig. 3 are the drain current and voltage waveforms of the main circuit, simulated in ADS using the actual transistor's large-signal model. Here, the main and auxiliary circuits were biased with $V_{GG1} = -3.1$ V, $V_{DD1} = 28$ V, $V_{GG2} = -3.1$ V, and $V_{DD2} = 16.8$ V. The simulated peak drain voltage factor is 2.77 which is considerably lower than that of the Class-E_M in [8], i.e., 4.4. Moreover, Fig. 3 shows that the main circuit satisfies the Class-E_M/F_3 switching conditions, namely zero voltage switching (ZVS), zero voltage derivative switching (ZVDS), zero current switching (ZCS), and zero current derivative switching (ZCDS).

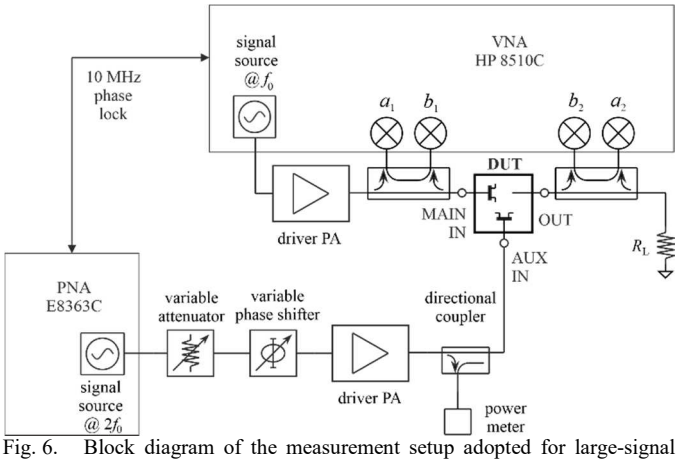


Fig. 6. Block diagram of the measurement setup adopted for large-signal characterization.

III. Implementation And Measurements

The designed Class-E_M/F_3 PA was fabricated on a 0.51-mm-thick RO4003C substrate with a dielectric constant of 3.38. The photograph of the circuit prototype is shown in Fig. 4. The PA prototype was first characterized under small-signal conditions using the Keysight E8363C PNA. The PA was biased with V_{GG1} = –2.9 V, V_{DD1} = 28 V, V_{GG2} = –2.75 V, and V_{DD2} = 16.8 V. The measured scattering parameters are depicted in Fig. 5, showing that the PA delivers a small-signal gain greater than 12 dB from 1.4 to 2 GHz. The large-signal characterization was performed using the measurement setup shown in Fig. 6, where a single-input real-time vector large-signal test bench based on the HP 8510C VNA was used to feed the main circuit with an input signal at f_0 and to measure the output power at the same frequency. The Keysight E8363C PNA was used as an additional signal source, phase-locked to the main signal source, to feed the auxiliary circuit with an input signal at $2f_0$. A variable attenuator and a variable phase shifter were added in the auxiliary input signal path for power and phase adjustments. The drain efficiency (*DE*) and power added efficiency (*PAE*) are defined as

$$DE = \frac{P_{out}}{P_{DC1} + P_{DC2}} \tag{1}$$

$$PAE = \frac{P_{out} - P_{inM} - P_{inA}}{P_{DC1} + P_{DC2}} \tag{2}$$

The measured performances of the PA are depicted in Fig. 7, with Fig. 7(a) showing the measured gain, *DE*, and *PAE* versus the output power at 1.8 GHz. The PA delivers a gain of 11.5 dB, a *DE* of 77%, and a *PAE* of 72% at a peak P_{out} of 42.1 dBm. Moreover, at 6-dB OBO, the PA delivers a gain of 14 dB, a *DE* of 41%, and a *PAE* of 40%. Fig. 7(b) shows that the PA delivers *DE* > 67%, *PAE* > 58%, a P_{out} of 41.2 ± 1 dBm, and power gain > 7.3 dB over a 600 MHz frequency range which corresponds to a 34.3% fractional bandwidth (FBW) which is greater than the typical 10-15% FBW of the traditional switching PAs.

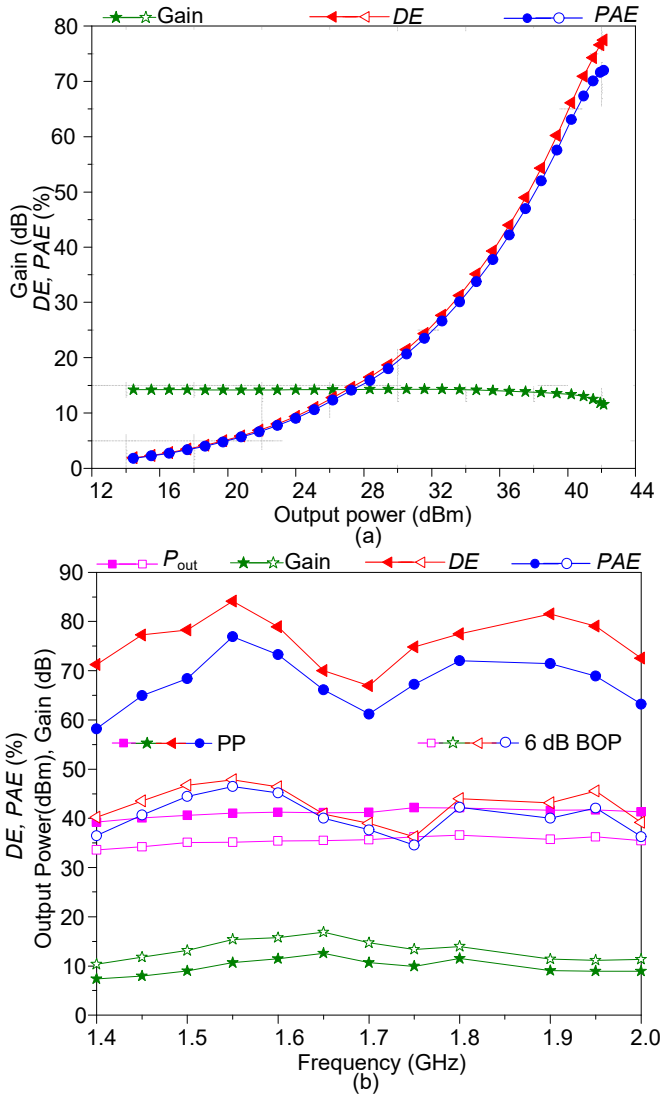


Fig. 7. Measured performances (a) versus output power at 1.8 GHz. (b) versus frequency at peak output power and 6-dB back-off.

More importantly, Fig. 7(b) shows that at 6 dB OBO, the PA delivers *DE* > 39%, *PAE* > 34%, a P_{out} of 35 ± 1.2 dBm, and power gain > 10 dB over a 600 MHz frequency range.

It is worth noting that the impedance matching between R_L and Z_{opt} at f_0 is only performed by the combined series lines TL_2 + TL_4 and the stubs TL_{5A} + TL_{5B} since TL_{3A} + TL_{3B} behaves like an open circuit at f_0. With $\theta_4 = \lambda/8$ at f_0, the combined series lines TL_2 + TL_4 form a frequency selective quarter-wave transformer. The broadband response in Fig. 7(b) results from the resistive-reactive impedance at $2f_0$ imposed by the second-harmonic current injected from the auxiliary circuit into the main circuit.

IV. Conclusion

The design of a high-efficiency Class-E_M/F_3 power amplifier with a reduced peak drain voltage and a large fractional bandwidth of 34.3% at both peak power and 6 dB back-off power has been presented and verified through the

implementation of a GaN HEMTs PA prototype operating from 1.4 to 2 GHz. The performances of the PA are summarized in Table I and compared with other pertinent GaN PA variants, namely harmonic-injection PAs and Doherty PAs. Table I shows that the bandwidth performance at peak power compares well with other harmonic-injection PAs while the bandwidth performance at 6-dB back-off compares well with Doherty PAs.

TABLE I
PERFORMANCE SUMMARY AND COMPARISON WITH OTHER GAN PAS

Ref.	Variant	Frequency (GHz)	P_{SAT} (dBm)	DE_{PP} (%)	DE_{BOP} (%)
[10]	Harmonic injection	0.88-1.06	40-41.6	84-94	-
[11]	Harmonic injection	1-1.9	40.2-42.6	60-71	-
[12]	Doherty	1.1-2.4	43.3	55-86	44-55
[13]	Doherty	2.1-2.66	43	57-84	39-67
This work	Class-E_M/F_3	1.4-2	39.2-42.1	67-84	36-49

ACKNOWLEDGMENT

This work was supported by the UK Engineering and Physical Sciences Research Council (EPSRC) under Grant EP/P013031/1.

REFERENCES

[1] N. O. Sokal and A. D. Sokal, "Class E – A new class of high-efficiency tuned single-ended switching power amplifiers," *IEEE J. Solid-State Circuits*, vol. 10, no. 3, pp. 168-176, Jun. 1975.

[2] T. Mury and V. F. Fusco, "Series-L/parallel-tuned comparison with shunt-C/series-tuned Class-E power amplifier," *IEE Proc. Circuits Devices Syst.*, vol. 152, no. 6, pp. 709-717, Dec. 2005.

[3] F. H. Raab, "Class-F power amplifiers with maximally flat waveforms," *IEEE Trans. Microw. Theory Techn.*, vol. 45, no. 11, pp. 2007-2012, Nov. 1997.

[4] T. Sharma, *et al*. "Simplified first-pass design of high-efficiency Class-F^{-1} power amplifiers based on second harmonic minima," *IEEE Trans. Microw. Theory Techn.*, vol. 67, no. 7, pp. 3147–3161, Jul. 2019.

[5] V. Carrubba, J. Lees, J. Benedikt, P. J. Tasker, and S. C. Cripps, "A novel highly efficient broadband continuous class-F RFPA delivering 74% avarage efficiency for an octave bandwidth," *2011 IEEE MTT-S Int. Microw. Symp. (IMS)*, Baltimore, MD, USA, 2011, pp. 1–4.

[6] E. Aggrawal, K. Rawat, and P. Roblin, "Investigating continuous Class-F power amplifier using nonlinear embedding model," *IEEE Microw. Compon. Lett.*, vol. 27, no. 6, pp. 593–595, Jun. 2017.

[7] C. Friesicke, R. Quay, and A. F. Jacob, "The resistive-reactive Class-J power amplifier mode," *IEEE Microw. Compon. Lett.*, vol. 25, no. 10, pp. 666–668, Oct. 2015.

[8] M. S. Mugisho, M. Thian, and A. Grebennikov, "Broadband Class-E_M power amplifier with double reactance compensation technique," *2020 IEEE Int. Symp. Circuts Syst. (ISCAS)*, Seville, Spain, 2020, pp. 1-5.

[9] M. S. Mugisho, N. Buchanan, M. Thian, and A. Grebennikov, "Harmonic-injection Class-E_M/F_3 power amplifier with finite dc-feed inductance," *2020 IEEE International Workshop on Integrated Nonlinear Microwave and Millimetre-Wave Circuits* (*INMMiC*), Cardiff, United Kingdom, 2020, pp. 1-3.

[10] M. Seo, *et al*. "High-efficiency power amplifier using an active second-harmonic injection technique under optimized third-harmonic termination," *IEEE Trans. Circuits Syst. II, Exp. Briefs*, vol. 61, no. 8, pp. 549-553, Aug. 2014.

[11] Y. M. A. Latha, K. Rawat, M. Helaoui, and F. M. Ghannouchi, "Broadband continuous mode power amplifier with on-board harmonic injection," *IET Microw. Antennas Propag.*, vol. 13, no. 9, pp. 1402-1407, Jul. 2019.

[12] Z. Yang *et al*., "Bandwidth extension of Doherty power amplifier using complex combining load with noninfinity peaking impedance," *IEEE Trans. Microw. Theory Techn.*, vol. 67, no. 2, pp. 765-777, Feb. 2019.

[13] A. Barakat, M. Thian, V. Fusco, S. Bulja and L. Guan, "Toward a more generalized Doherty power amplifier design for broadband operation," *IEEE Trans. Microw. Theory Techn.*, vol. 65, no. 3, pp. 846-859, Mar. 2017.